

# Catastrophic Sliding Bifurcations, & onset of oscillations in a superconducting resonator

M. R. Jeffrey\* and A. R. Champneys

*BCANM, Engineering Mathematics Department, University of Bristol BS8 1TR*

M. diBernardo

*BCANM, Engineering Mathematics Department, University of Bristol BS8 1TR and*

*Department of Systems and Computer Science,*

*University of Naples Federico II, Via Claudio 21, 80125, Napoli, Italy*

S. W. Shaw

*Department of Mechanical Engineering,*

*Michigan State University, East Lansing, MI 48824-1226 USA*

(Dated: December 18, 2009)

This paper presents a general analysis and a concrete example of the catastrophic case of a discontinuity-induced bifurcation in so-called Filippov nonsmooth dynamical systems. Such systems are characterised by discontinuous jumps in the right-hand-sides of differential equations across a phase space boundary and are often used as physical models of stick-slip motion and relay control. Sliding bifurcations of periodic orbits have recently been shown to underlie the onset of complex dynamics including chaos. In contrast to previously analysed cases, in this work a periodic orbit is assumed to graze the boundary of a repelling sliding region, resulting in its abrupt destruction without any pre-cursive change in its stability or period. Necessary conditions for the occurrence of such catastrophic grazing-sliding bifurcations are derived. The analysis is illustrated in a piecewise-smooth model of a stripline resonator, where it can account for the abrupt onset of self-modulating current fluctuations. The resonator device is based around a ring of NbN containing a microbridge bottleneck, whose switching between normal and superconducting states can be modelled as discontinuous, and whose fast temperature versus slow current fluctuations are modeled by a slow-fast timescale separation in the dynamics. By approximating the slow component as Filippov sliding, explicit conditions

are derived for catastrophic grazing-sliding bifurcations, which can be traced out as parameters vary. The results are shown to agree well with simulations of the slow-fast model and to offer a simple explanation of one of the key features of this novel experimental device.

## I. INTRODUCTION

An increasing number of physical devices in applied science and engineering are modeled using sets of ordinary differential equations with discontinuous right-hand sides. Examples include mechanical impacts [1] or stick-slip motion from friction [2], electronic switches [3, 4], hybrid dynamics in control [5], and genetic networks [6]. Overviews and further references are available in [7–10].

A particular class of interest is that of so-called *Filippov systems* [11], where it is typical for trajectories to become constrained to a discontinuity boundary in phase space, called *sliding*, resulting in a loss of uniqueness of solutions. It has been observed that complex dynamical transitions can occur when so-called *sliding bifurcations* take place; namely, when the system trajectory interacts nontrivially with a discontinuity boundary in phase space where attracting sliding motion is possible. Sliding bifurcations in Filippov systems have been observed to cause dramatic transitions in the dynamics of several systems of relevance in applications.

In [8, 12], a heuristic classification of sliding bifurcations was presented where four fundamental scenarios were outlined: grazing-sliding, crossing-sliding, adding-sliding and switching-sliding. In all cases, analytical defining conditions were given together with appropriate non-degeneracy conditions to define each of the cases proposed. A summarising schematic of these four cases is shown in Figure 1. By means of appropriate discontinuity-mappings, the simplest possible scenarios associated to each of these bifurcation events was classified, showing that in general periodic orbits undergoing these bifurcations will locally persist, acquiring an extra segment with sliding motion. The most dramatic scenario is that associated to the grazing-sliding of a periodic orbit, which was shown analytically to

---

\*Electronic address: [mike.jeffrey@bristol.ac.uk](mailto:mike.jeffrey@bristol.ac.uk)

correspond to a non-invertible piecewise linear Poincaré map. Under certain condition this can lead, for example, to the sudden transition from periodic attractors to chaos as shown in [13] for the case of a nonlinear friction oscillator.

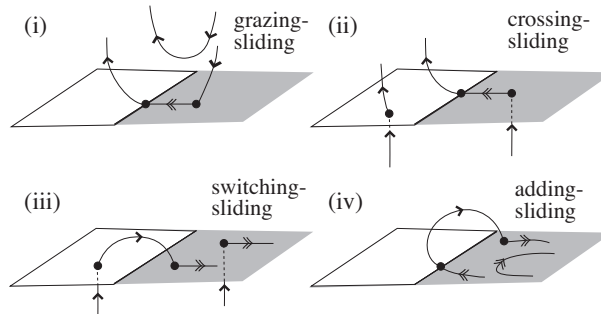


FIG. 1: Phase portraits for the four sliding bifurcations in three dimensions. The discontinuity manifold is represented by a horizontal plane in which the attracting sliding region is shaded.

The four cases in Figure 1 all occur at the boundary of an attracting sliding region – the discontinuity manifold attracts trajectories from the surrounding phase space, causing nonuniqueness of solutions in reverse time. In contrast, this paper presents a novel sliding bifurcation scenario we refer to as *catastrophic grazing-sliding*, characterized by a trajectory interacting with the boundary of a repelling sliding region. A repelling sliding region is unstable in finite time, and consists of sliding solutions that are nonunique in forward time (illustrated in Figure 2, section II B).

Catastrophic sliding bifurcations have arisen from attempts to provide a complete classification of sliding bifurcations [14]; they occur when a nontrivial interaction between a trajectory and a phase space boundary cause the sudden appearance/disappearance of a periodic orbit. Nevertheless, as we shall show, interaction with the boundary of a repelling sliding region leads in many cases to a well defined bifurcation scenario, characterized by a finite jump in attractor to a new region of phase space without any incipient exponential instability being detectable. In some sense then, catastrophic sliding bifurcations are the most abrupt form of “blue sky catastrophe” [15] in that, from the point of view of the orbit prior to the bifurcation, there is no warning of the impending catastrophe.

The main result of the paper is in section II B, where we give the analytical defining conditions for a catastrophic grazing-sliding bifurcation to occur. Then we use the theoretical results to explain transitions recently observed in an experimental superconducting stripline

resonator [16]. This system was studied extensively in [16–19]. It was observed that parameter variations caused the sudden disappearance of certain periodic orbits. Because of its physical nature, it has become clear that features of the stripline resonator can be modelled as a piecewise-smooth dynamical system (switching at a fixed temperature) combined with a slow-fast system (two slow invariant parabolas) [18].

Here we show that the discontinuous nature of the idealized model can be used to explain the sudden disappearance of periodic orbits by means of a catastrophic grazing-sliding bifurcation. In so doing we simplify the model, which consists of a nonlinear piecewise-smooth vector field and two slow invariant manifolds, to a linear Filippov system where the slow manifolds are replaced by discontinuity boundaries.

We show that fixed points in the sliding flow occur at the same values of variables and parameters as in the original system, and, importantly, that periodic orbits graze a discontinuity boundary in both systems also at the same values. This allows us to find a transcendental equation for periodic orbits, from which the exact parameters at which catastrophic grazing occur can be numerically determined. Numerical simulations are used to validate the theoretical analysis. Both the numerics and the analysis fit the experimental observations of [16, 18], confirming the discontinuous nature of the bifurcation scenario causing the disappearance of the periodic orbit. Moreover, we are able to trace precisely the loci of such catastrophic bifurcations.

The rest of the paper is organised as follows. In Section II we outline the four familiar bifurcations of periodic orbits related to sliding, and present our main subject – a catastrophic bifurcation – for which we provide a definition and existence conditions. We then introduce our case study, the superconducting stripline resonator, in Section III A. The model of this is given in Section III B, and in equation (8) we derive a dimensionless form for analytical study. This is simplified to a piecewise-linear system in Section III C, from which we derive periodic orbits and limit cycles in Section IV, including the conditions for catastrophic bifurcations for the model in Section IV C. We complement this analysis with numerically computed bifurcation diagrams and simulations in Section V. Some closing remarks are given in Section VI, including a comparison of simulations to a smoothed version of the original slow-fast model.

## II. SLIDING BIFURCATIONS

The qualitative change of a dynamical system caused by the interaction of some invariant set with a discontinuity manifold is called a *discontinuity-induced bifurcation* [8]. A discontinuity manifold is a smooth hypersurface where the state of a system or its derivative jumps. In a Filippov system [11], the dynamics is defined on the manifold by a differential inclusion (see next section). Two important discontinuity-induced phenomena are *boundary-equilibrium bifurcations*, where a stable fixed point of a flow meets a discontinuity manifold, and *grazing bifurcations*, where a periodic orbit meets a discontinuity manifold tangentially, and we say it *grazes*.

Grazing occurs generically in discontinuous systems. It leads, for example, to robust chaos with period adding windows in maps [20, 21], and to transitions from periodic to chaotic attractors in impact oscillators [22, 23]. In a dry-friction system, grazing causes the onset of sticking [24] whereby a periodic orbit sticks to the switching manifold. When such transitions occur due to grazing, that is, when periodic orbits lose or gain points of interaction with a discontinuity boundary that contains sliding, we call them *sliding bifurcations*.

### A. The four attracting sliding bifurcations

The four well-known cases of sliding bifurcations in piecewise-smooth (Filippov) systems are shown in Figure 1. These importantly take place at the boundary between an attracting sliding region (where the flows either side of the discontinuity manifold tend towards it) and a crossing region (through which orbits cross the manifold), with the result that a periodic orbit typically persists through the bifurcation. The persistence of the periodic orbit can be proven by the derivation of a return map to an appropriate section through phase space, two natural choices being the zero-time discontinuity mapping and Poincaré discontinuity mapping [8, 12].

The bifurcation termed grazing-sliding, in Figure 1(i), is of particular interest, because it occurs when the periodic orbit of a smooth subsystem grazes at the boundary of attracting sliding. Hereafter we are concerned with an event suggested by numerical simulations in [8] and a generic classification scheme in [14], namely that when a periodic orbit grazes a discontinuity boundary with repelling sliding, the resulting bifurcation is catastrophic.

## B. Catastrophic sliding bifurcations

As catastrophic sliding bifurcations are not well known, we will provide a full definition of them in this section.

A sliding bifurcation can be analyzed by considering the geometry of phase space in the neighbourhood of grazing. Let us consider a dynamical system of the form

$$\dot{x} = \begin{cases} f_1(x), & \text{if } h(x) > 0, \\ f_2(x) & \text{if } h(x) < 0, \end{cases} \quad (1)$$

comprised of smooth vector fields  $f_1$ ,  $f_2$ , and a discontinuity boundary defined implicitly as  $\Sigma = \{x \in \mathbb{R}^n : h(x) = 0\}$ , henceforth referred to as a *switching manifold*. The dynamics on the manifold is prescribed in the Filippov convention [11] as follows. Let  $\mathcal{L}_f$  denote the Lie derivative along the flow of a vector field  $f$ , that is,  $\mathcal{L}_f = f \cdot \nabla h$ . Then orbits cross through  $\Sigma$  if  $(\mathcal{L}_{f_1}h)(\mathcal{L}_{f_2}h) > 0$ . *Attracting sliding* occurs in a region on  $\Sigma$  where  $\mathcal{L}_{f_1}h < 0 < \mathcal{L}_{f_2}h$ , where sliding trajectories evolve along the manifold as solutions of  $\dot{x} = F$ , with

$$F = \frac{(\mathcal{L}_{f_2}h)f_1 - (\mathcal{L}_{f_1}h)f_2}{(\mathcal{L}_{f_2}h - \mathcal{L}_{f_1}h)} \quad (2)$$

being simply the member of the convex combination of  $f_1$  and  $f_2$  that is tangent to the switching manifold (Figure 2). The sliding bifurcations in Figure 1 occur at the boundary between crossing and attracting sliding regions, where  $\mathcal{L}_{f_1}h = 0 < \mathcal{L}_{f_2}h$  or  $\mathcal{L}_{f_2}h = 0 > \mathcal{L}_{f_1}h$ .

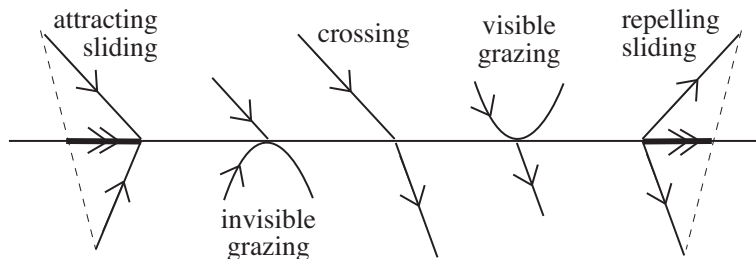


FIG. 2: A Filippov system, depicting the different types of dynamics that occur at a switching manifold: attracting or repelling sliding (double arrows show sliding vector field), and crossing. At the boundaries between sliding and crossing, trajectories graze the switching manifold.

A less studied scenario is the *repelling sliding* that occurs on  $\Sigma$  where  $\mathcal{L}_{f_2}h < 0 < \mathcal{L}_{f_1}h$ . Here we can apply the vector field  $F$ , but any infinitesimal perturbation would cause a

trajectory immediately to depart the neighbourhood of  $\Sigma$ . A consequence of this instability is that grazing at the boundary of a repelling sliding region will be catastrophic, in the sense that a periodic orbit may be suddenly destroyed by a small change in a parameter. The boundary between crossing and repelling sliding satisfies one of the conditions  $\mathcal{L}_{f_1}h = 0 > \mathcal{L}_{f_2}h$  or  $\mathcal{L}_{f_2}h = 0 < \mathcal{L}_{f_1}h$ .

Contrast the grazing-sliding bifurcation in Figure 1 with the scenario in Figure 3. Each pair of trajectories depict the local portrait of a grazing periodic orbit after a small perturbation. In the latter case the trajectory cannot return to the upper region after interacting with the manifold without exiting the local neighbourhood. As a result, no local return map can be defined that exists throughout the bifurcation and a periodic orbit will not persist.

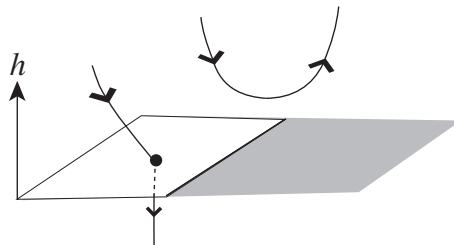


FIG. 3: A periodic orbit above the switching manifold  $h = 0$  is destroyed by a catastrophic grazing-sliding bifurcation. The local phase portrait is shown with the sliding region shaded.

Thus we have the following necessary conditions for catastrophic grazing-sliding, at the bifurcation point:

$$\text{either } \mathcal{L}_{f_1}h = 0 \text{ and } \mathcal{L}_{f_2}h < 0 < \mathcal{L}_{f_1}(\mathcal{L}_{f_1}h), \quad (3)$$

$$\text{or } \mathcal{L}_{f_2}h = 0 \text{ and } \mathcal{L}_{f_1}h > 0 > \mathcal{L}_{f_2}(\mathcal{L}_{f_2}h). \quad (4)$$

The conditions (3) and (4) respectively imply grazing from above ( $h > 0$ ) or below ( $h < 0$ ) the switching manifold  $\Sigma$ , and the inequalities are nondegeneracy conditions which mean the following. In (3),  $\mathcal{L}_{f_1}(\mathcal{L}_{f_1}h) > 0$  specifies that grazing orbits above  $\Sigma$  curve quadratically (because it is nonzero) away (because it is positive) from  $\Sigma$ , while  $\mathcal{L}_{f_2}h < 0$  guarantees that  $f_2$  points away from  $\Sigma$  and does not graze. The conditions (4) similarly mean that orbits below  $\Sigma$  graze quadratically while  $f_1$  points away from  $\Sigma$ . When an orbit curves away from the manifold we say it is *visibly grazing*, see Figure 2 (invisible grazing means the orbit curves towards the manifold). The set of points satisfying (3) or (4) form a boundaries on  $\Sigma$  between crossing and repelling sliding.

We turn now to an example of this catastrophic grazing-sliding bifurcation in the model of a superconducting stripline resonator. In this piecewise-smooth model, an annular strip of repelling sliding on the switching manifold is surrounded by regions of crossing, providing two boundaries where catastrophic bifurcations take place. We will see that a periodic orbit is destroyed through grazing the system evolves towards a pair of stable attractors, which themselves undergo boundary-equilibrium bifurcations nearby in parameter space.

### III. THE RESONATOR MODEL

#### A. System Description

The physical system of interest consists of a circular ring of niobium nitride (NbN), typically a few centimetres in circumference with a cross-section on the order of several square microns, see Figure 4(i-ii) and [16–19]. The ring is immersed in a liquid helium bath so that it becomes superconducting. Electromagnetic waves are excited in the ring using a harmonic voltage applied through a feedline, and the response is measured by the signal reflected at the point of input. The forcing frequency  $\omega_p$  is taken to be near an electromagnetic mode of the ring, whose first few natural frequencies are on the order of 1-10GHz. A key feature of the system is that it has a small microbridge of very narrow cross-section that acts like a bottleneck for the current in the ring (Figure 4(ii)). This microbridge is annularly located so that it sees a large current in the mode of interest, and thus the impedance of the microbridge dominates that of the entire ring. These devices were developed so that one could rapidly alter the resonance frequency of the ring by manipulating the impedance of the microbridge by shining a laser on it [16]. In the course of exploring the system response, some unexpectedly rich dynamics were observed, as described below.

Typically the system acts as a resonator with linear response dominated by a single mode. For example, this holds if the driving amplitude is small and/or far from resonance, in which case the entire ring remains superconducting. Similarly, if the driving input is sufficiently large, Joule heating prevents the microbridge from ever being superconducting, and the system again behaves like a linear resonator, albeit with different response characteristics, due to the different microbridge impedance. In the following, we describe the response of the resonant mode of interest as  $B(t)e^{-i\omega_p t}$ , where the complex variable  $B$  captures the slowly

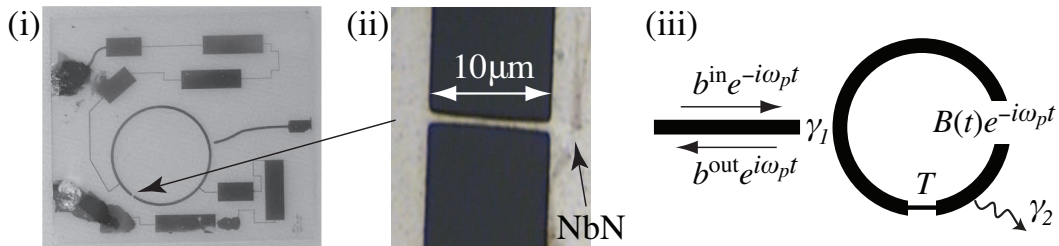


FIG. 4: (i) Image of the resonator device showing the NbN ring, and (ii) optical microscope (inverted color) image of the microbridge in the ring [provided courtesy of Eran Segev and Eyal Buks]. (iii) Schematic model of the device showing the driving amplitude  $b^{\text{in}}$  and frequency  $\omega_p$ , the response  $B(t)e^{-i\omega_p t}$  of the resonator, and the temperature  $T$  of the microbridge [16].

varying amplitude and phase of the modal response, and  $\omega_p$  is the forcing frequency. This is shown schematically in Figure 4(iii). The interesting dynamics occur when the microbridge switches between normal and superconducting, with different impedance characteristics in either mode. The other dynamic state in the model is the microbridge temperature  $T$ , which dictates its impedance. If  $T < T_C$ , where  $T_C$  is the critical temperature of NbN (on the order of 10 Kelvin), the impedance is that of the superconducting state, denoted  $S$ , whereas when  $T > T_C$  the microbridge becomes normal conducting, denoted  $N$ , in which case it has much greater resistance and the ring may have slightly different resonant frequencies.

The key to understanding the rich dynamics observed for this system is to note that the microbridge temperature  $T$  depends on the local average current density in the microbridge, which is related to the modal amplitude  $|B|$  through Joule heating (and dissipation), and  $B$  in turn depends on the impedance in the ring (as well as the excitation parameters), and thus on  $T$ . If the excitation is moderately strong and near resonance, this coupling leads to a situation in which the current amplitude will grow and heat the microbridge until it becomes normal conducting, at which point the system becomes more highly damped (and possibly off resonance), resulting in a reduced amplitude. This then leads to a cooling of the microbridge, until it once again becomes superconducting. The resulting sustained oscillation of the system between these states was designated as “self-modulation” in [16], where a piecewise-smooth (in fact, piecewise linear) model was developed that accurately captured, via simulations, most of the experimentally observed behaviour; (it should be noted that noise plays an important role in the behaviour near some transitions, a feature

not addressed in the present work). The piecewise-smooth model exhibits different linear behaviours on either side of  $T_C$  (due to the change in microbridge impedance), and also exhibits relatively fast dynamics in  $T$  when compared to those in  $B$  (due to the very low levels of dissipation and the fact that the system is driven near resonance). The purpose of the present paper is to show that this simple model for the coupled  $(B, T)$  dynamics has a periodic orbit that describes the self-modulation, and that it is created/destroyed by catastrophic grazing bifurcations. These bifurcations occur independent of, but are strongly influenced by, conditions for the creation and destruction of the fixed points that correspond to the periodic resonant behaviours that remain entirely in either N or S.

In the next section we present the idealized model of this system derived in [16, 17]. Of course, the transition between N and S is complicated and not instantaneous, but it does occur quickly compared to the time scale of the response, and can therefore be conveniently modeled as an immediate switch between N and S states across  $T_C$ ; this is the ultimate source of the piecewise-smooth nature of the following model.

## B. Piecewise-smooth model

The model for the resonator is the dynamical system

$$\begin{aligned}\dot{B} &= [i(\omega_p - \omega_0(T)) - \gamma_1 - \gamma_2(T)] B - i\sqrt{2\gamma_1} b^{\text{in}} \\ \dot{T} &= g[(T_0 - T) + 2\kappa\hbar\omega_0\gamma_2(T)|B|^2/H].\end{aligned}\tag{5}$$

The first equation describes the complex amplitude  $B$  of a harmonically driven oscillator, and is essentially linear in character, except for the fact that the natural frequency and damping depend on the temperature  $T$ . These coefficients are piecewise constant and take on different values depending on whether  $T$  is above or below  $T_C$ . The  $T$  dynamics are driven by linear decay that drives the temperature to the bath temperature  $T_0$ , described by the first term, while the second term captures the  $B$ -dependent Joule heating in the microbridge.

Note that  $g = H/C$  is a large parameter which implies fast dynamics evolving towards slow manifolds where  $\dot{T} = 0$ . Here  $H$  is a heat transfer coefficient between the resonator microbridge with thermal heat capacity  $C$  and a coolant with temperature  $T_0$ . Several parameters depend on whether the NbN is normal or superconducting:  $\kappa$  measures efficiency

of microbridge heating relative to power dissipated and is typically estimated to be near one,  $\omega_0$  is the angular resonance frequency,  $\gamma_1$  is the coupling coefficient between the resonator and feedline, and  $\gamma_2$  is the damping rate of the mode (see Figure 4(iii)). The symbol  $i$  is the imaginary unit  $\sqrt{-1}$ .

Typical values of the main parameters are shown in Table I. The only physical parameters that will recur in this paper, for producing a bifurcation diagram in Figure 8, are the driving frequency  $\omega_p$ , and the driving amplitude  $b^{\text{in}}$  providing a pump power proportional to  $|b^{\text{in}}|^2$  (for simplicity we let  $b^{\text{in}}$  be real without qualitatively changing our results).

TABLE I: Values of the physical parameters of the model in the typical operating range of the resonator device [16–18].

parameter	typical value range
$\omega_0$	20 – 30GHz, $\omega_{0S} < \omega_{0N}$
$\gamma_1/\omega_0$	0.001 – 0.25
$\gamma_2/\omega_0$	0.002 – 0.6, $\gamma_{2S} \ll \gamma_{2N}$
$\omega_p/\omega_0$	0.98 – 1.02
$g/\omega_0$	4 – 8
$\kappa$	$0 < \kappa \lesssim 1$

For analysis it is convenient to transform to dimensionless state variables  $\beta = \frac{g}{\sqrt{2}\gamma_1 b^{\text{in}}} B$  and  $\Theta = \frac{T-T_0}{T_C-T_0}$ , such that  $\Theta = 0$  is the bath temperature and  $\Theta = 1$  is the transition temperature between N and S modes. We define dimensionless parameters

$$\Lambda = \frac{1}{g} [i(\omega_p - \omega_0) - \gamma_1 - \gamma_2], \quad \sigma = \frac{4\kappa\hbar\omega_0\gamma_1\gamma_2}{g^3 C(T_C - T_0)}, \quad (6)$$

such that  $\Lambda$  is a complex coefficient describing the driven linear oscillator dynamics, and  $\sigma$  describes the effective Joule heating. Both take on different values for  $T > T_C$  and  $T < T_C$ . Note that large  $g$  implies  $\sigma \ll |\Lambda| \ll 1$ . The physical parameter values in Table I imply that

$$\text{Re}\Lambda < 0 \quad \text{and} \quad \sigma_N > \sigma_S. \quad (7)$$

We thus obtain a two-parameter system

$$\begin{aligned} \dot{\beta} &= \Lambda(\Theta)\beta - i \\ \dot{\Theta} &= -\Theta + \sigma(\Theta)|\beta|^2, \end{aligned} \quad (8)$$

where the dot now indicates differentiation with respect to  $\tau = gt$ . Then  $\sigma$  and  $\Theta$  are real whereas  $\Lambda$  and  $\beta$  are complex. The parameters are piecewise-constants that jump at  $\Theta = 1$ , specified as

$$\Lambda(\Theta) = \begin{cases} \Lambda_{\mathbf{N}} & \text{if } \Theta > 1, \\ \Lambda_{\mathbf{S}} & \text{if } \Theta < 1, \end{cases} \quad \text{and} \quad s(\Theta) = \begin{cases} \sigma_{\mathbf{N}} & \text{if } \Theta > 1, \\ \sigma_{\mathbf{S}} & \text{if } \Theta < 1. \end{cases} \quad (9)$$

The system (8) is therefore piecewise-smooth: smooth in the region  $\Theta > 1$  labelled **N** and the region  $\Theta < 1$  labelled **S**, separated by a switching manifold defined by  $\Theta = 1$ .

For  $\sigma \ll |\Lambda| \ll 1$ , each subsystem **N** and **S** has slow-fast dynamics. The theory of normally hyperbolic invariant manifolds [25] applied away from  $\Theta = 1$  can be used to show that a slow invariant manifold exists close to the surfaces where  $\dot{\Theta} = 0$ . The slow manifolds are two-dimensional paraboloids in the  $(\beta, \Theta)$  phase space (shown later in Figure 6(i)), which are given by  $\Theta = \sigma_{\mathbf{N}} |\beta|^2$  for  $\Theta > 1$  and  $\Theta = \sigma_{\mathbf{S}} |\beta|^2$  for  $\Theta < 1$ . The fast dynamics of  $\Theta$  imply that the system evolves quickly into a neighbourhood  $|\Theta - \sigma_{\mathbf{N,S}} |\beta|^2| < \epsilon$  of the attractive invariant manifolds, for some small  $\epsilon > 0$ .

In the following we approximate the dynamics of (8) with a Filippov model that can be solved explicitly. We do so by approximating the vector field with its value at the boundaries of the  $\epsilon$ -neighbourhood of the slow invariant manifolds, given by  $|\Theta - \sigma_{\mathbf{N,S}} |\beta|^2| = \epsilon$ , which means setting  $\dot{\Theta} = -\epsilon \text{sign}[\Theta - \sigma(\Theta) |\beta|^2]$ . The dynamics will not rely critically on the choice of  $\epsilon$ , for instance, the algebraic expression for periodic orbits and equilibria will not depend on  $\epsilon$  at all.

### C. A Filippov resonator model

The preceding arguments suggest the following piecewise-linear system:

$$\begin{pmatrix} \dot{\beta} \\ \dot{\Theta} \end{pmatrix} = \begin{pmatrix} \Lambda(\Theta) \beta - i \\ -\epsilon \text{sign}(h) \end{pmatrix}, \quad (10)$$

written in terms of the complex piecewise-constant

$$\Lambda(\Theta) = \begin{cases} \Lambda_{\mathbf{N}} & \text{if } \Theta > 1, \\ \Lambda_{\mathbf{S}} & \text{if } \Theta < 1, \end{cases} \quad (11)$$

and the switching function

$$h(\beta, \Theta) = \begin{cases} h_{\mathbf{N}}(\beta, \Theta) & \text{if } \Theta > 1, \\ h_{\mathbf{S}}(\beta, \Theta) & \text{if } \Theta < 1, \end{cases} \quad (12)$$

where

$$h_r(\beta, \Theta) = \Theta - \sigma_r |\beta|^2, \quad (13)$$

with  $\epsilon$  a small positive constant. This means that state space is partitioned by three switching manifolds,

$$\Sigma = \{(\beta, \Theta) : \Theta = 1\}, \quad (14)$$

$$\Sigma_{\mathbf{N}} = \{(\beta, \Theta) : \Theta > 1, h_{\mathbf{N}} = 0\}, \quad (15)$$

$$\Sigma_{\mathbf{S}} = \{(\beta, \Theta) : \Theta < 1, h_{\mathbf{S}} = 0\}. \quad (16)$$

Explicitly we have four regions  $\mathbf{N1}$ ,  $\mathbf{N2}$ ,  $\mathbf{S1}$ ,  $\mathbf{S2}$ , and the dynamical system

$$\begin{pmatrix} \dot{\beta} \\ \dot{\Theta} \end{pmatrix} = \begin{cases} f_{\mathbf{N1}} & \text{if } \Theta > 1, h_{\mathbf{N}} > 0, \\ f_{\mathbf{N2}} & \text{if } \Theta > 1, h_{\mathbf{N}} < 0, \\ f_{\mathbf{S1}} & \text{if } \Theta < 1, h_{\mathbf{S}} > 0, \\ f_{\mathbf{S2}} & \text{if } \Theta < 1, h_{\mathbf{S}} < 0, \end{cases} \quad (17)$$

where

$$f_{r1} = \begin{pmatrix} \Lambda_r \beta - i \\ -\epsilon \end{pmatrix} \quad \text{and} \quad f_{r2} = \begin{pmatrix} \Lambda_r \beta - i \\ +\epsilon \end{pmatrix} \quad (18)$$

for  $r = \mathbf{N}, \mathbf{S}$ , as illustrated in Figure 5. The  $\Sigma$  plane contains two crossing regions  $|\beta|^2 < 1/\sigma_{\mathbf{N}}$  and  $|\beta|^2 > 1/\sigma_{\mathbf{S}}$  (where orbits cross it in the negative and positive  $\Theta$  directions respectively), and these are separated by an annular region  $1/\sigma_{\mathbf{N}} \leq |\beta|^2 \leq 1/\sigma_{\mathbf{S}}$  of repelling sliding (where both vector fields are directed away from  $\Sigma$ ).

According to the Filippov method, the ‘slow’ dynamics on the parabolas  $\Sigma_r$  is prescribed by the sliding vector fields for each region,

$$\begin{pmatrix} \dot{\beta} \\ \dot{\Theta} \end{pmatrix} = \begin{cases} F_{\mathbf{N}} & \text{if } \Theta > 1, \\ F_{\mathbf{S}} & \text{if } \Theta < 1, \end{cases} \quad (19)$$

where the  $F_r$  are given by (see equation (2))

$$F_r = \frac{(\nabla h_r \cdot f_{r2}) f_{r1} - (\nabla h_r \cdot f_{r1}) f_{r2}}{\nabla h \cdot (f_{r2} - f_{r1})} = \begin{pmatrix} \Lambda_r \beta - i \\ \sigma_r \text{Re}[\beta^*(\Lambda_r \beta - i)] \end{pmatrix}, \quad (20)$$

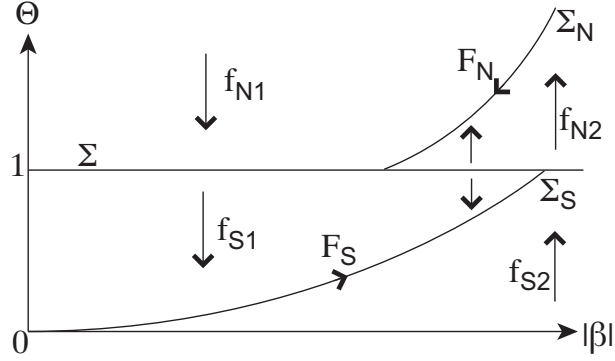


FIG. 5: Vector fields  $f_{N1}$ ,  $f_{N2}$ ,  $f_{S1}$ ,  $f_{S2}$ , apply in regions bounded by the planar switching manifold  $\Sigma$ , and the parabolic switching manifolds  $\Sigma_N$ ,  $\Sigma_S$  on which the sliding vector fields  $F_N$ ,  $F_S$  apply.

(note that this is the same as the vector field that would be obtained by taking the limit  $g \rightarrow \infty$  in (5) and setting  $F_r$  to be the vector field of the slow subsystem, often called the ‘reduced’ problem; because our interest is in using the model for illustrative purposes, we do not pursue this fact here). The sliding vector fields  $F_r$  apply only in the sliding regions

$$\Sigma_r^{\text{sl}} = \{(\beta, \Theta) : (\nabla h_r \cdot f_{r1}) (\nabla h_r \cdot f_{r2}) < 0\}; \quad (21)$$

otherwise orbits cross through the switching manifolds  $\Sigma_N$ ,  $\Sigma_S$ , and  $\Sigma$ , continuously but nondifferentiably.

On each parabola either side of  $\Sigma$ , the exactly solvable system (19) has the solution

$$\beta_r(\tau) - \frac{i}{\Lambda_r} = \left( \beta_{r0} - \frac{i}{\Lambda_r} \right) e^{\Lambda_r \tau}, \quad (22)$$

where  $\beta_{r0} = \beta_r(0)$ . We will not need the  $\Theta$  solution since (22) fully determines trajectories on  $\Sigma_r$ . Note that  $\beta_r(\tau)$  is continuous but nonsmooth because it jumps between  $r = N$  and  $r = S$  whenever  $\beta_r(\tau)$  crosses  $|\beta_r| = 1/\sqrt{\sigma_r}$  (when  $\Theta(\tau)$  crosses  $\Theta = 1$  at the intersection of  $\Sigma_r$  with  $\Sigma$ ), as illustrated in Figure 6(i).

We can depict the system as evolving on two overlapping regions covering the complex  $\beta$  plane (see Figure 6(ii)): trajectories follow  $F_S$  inside the circle  $|\beta| = 1/\sqrt{\sigma_S}$ , and follow  $F_N$  outside the circle  $|\beta| = 1/\sqrt{\sigma_N}$ , switching from one flow to the other when they intersect the circular boundaries. Given  $\sigma_N > \sigma_S$  (from equation (7)), the two regions overlap on the annulus  $1/\sqrt{\sigma_N} < |\beta| < 1/\sqrt{\sigma_S}$  where either vector field may be applied depending on the value of  $\Theta$ . We will use this representation for simulations in Figure 9.

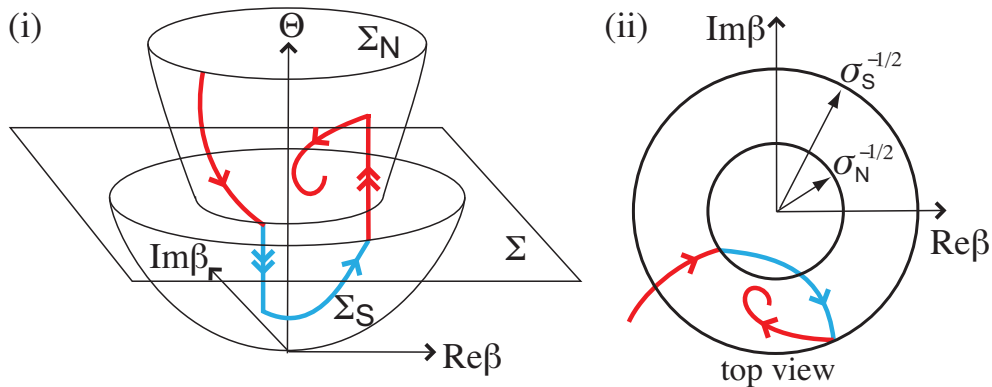


FIG. 6: (Color online) Example of an orbit of the Filippov system. (i) In the 3-dimensional phase space  $(\text{Re}\beta, \text{Im}\beta, \Theta)$ , orbits are attracted to and slide on the switching manifolds  $\Sigma_N$  and  $\Sigma_S$ , (ii) projection onto the complex  $\beta$  phase plane, showing intersections of the switching manifolds  $\Sigma_{N,S}$  with the switching manifold  $\Sigma$ . Fast dynamics are shown with double arrows, sliding orbits with single arrows.

#### IV. EQUILIBRIA AND LIMIT CYCLES

In this section we give equations of equilibria and necessary conditions for existence of periodic orbits in the Filippov model described in the previous section.

##### A. Conditions for equilibria

The sliding vector field (20) has equilibria, i.e.  $F_r = 0$ , at

$$\beta_r^{\text{eq}} = \frac{i}{\Lambda_r}. \quad (23)$$

An equilibrium in region N is admissible (lies in the region  $\Theta > 1$ ) if

$$|\Lambda_N|^2 < \sigma_N, \quad (24)$$

and an equilibrium in region S is admissible (lies in the region  $\Theta < 1$ ) if

$$|\Lambda_S|^2 > \sigma_S. \quad (25)$$

These relate the input power and frequency to the system parameters in a manner described more fully in Section V. Note that (23)-(25) are the same as for the original system (8). At these equilibria the Jacobian matrix of the sliding vector field has determinant  $|\Lambda_r|^2 > 0$  and eigenvalues equal to  $\Lambda_r$  and its complex conjugate. Hence, assuming from equation (7) that  $\text{Re}\Lambda_r < 0$ , each admissible equilibrium at  $\beta_r^{\text{eq}}$  is a stable focus in  $\Sigma_r$ .

## B. Conditions for periodic orbits

In principle we can find a transcendental expression that must be satisfied by periodic orbits in the Filippov model. We consider only periodic orbits that visit each region **N** and **S** precisely once per period. First rearrange (22) to express the time  $\tau$  spent in region  $r = \mathbf{N}$  or  $r = \mathbf{S}$  as

$$e^\tau = \left| \frac{\beta_r(\tau) - \frac{i}{\Lambda_r}}{\beta_0 - \frac{i}{\Lambda_r}} \right|^{\frac{1}{\operatorname{Re}\Lambda_r}}. \quad (26)$$

Substituting this expression back into (22) we obtain

$$\frac{\beta_r(\tau) - \frac{i}{\Lambda_r}}{\beta_0 - \frac{i}{\Lambda_r}} = \left| \frac{\beta_r(\tau) - \frac{i}{\Lambda_r}}{\beta_0 - \frac{i}{\Lambda_r}} \right|^{\frac{\Lambda_r}{\operatorname{Re}\Lambda_r}}. \quad (27)$$

Thus, a periodic orbit satisfies both of the conditions

$$\frac{\beta_{\mathbf{N}} - \frac{i}{\Lambda_{\mathbf{N}}}}{\beta_{\mathbf{S}} - \frac{i}{\Lambda_{\mathbf{N}}}} = \left| \frac{\beta_{\mathbf{N}} - \frac{i}{\Lambda_{\mathbf{N}}}}{\beta_{\mathbf{S}} - \frac{i}{\Lambda_{\mathbf{N}}}} \right|^{\frac{\Lambda_{\mathbf{N}}}{\operatorname{Re}\Lambda_{\mathbf{N}}}} \quad \text{and} \quad \frac{\beta_{\mathbf{S}} - \frac{i}{\Lambda_{\mathbf{S}}}}{\beta_{\mathbf{N}} - \frac{i}{\Lambda_{\mathbf{S}}}} = \left| \frac{\beta_{\mathbf{S}} - \frac{i}{\Lambda_{\mathbf{S}}}}{\beta_{\mathbf{N}} - \frac{i}{\Lambda_{\mathbf{S}}}} \right|^{\frac{\Lambda_{\mathbf{S}}}{\operatorname{Re}\Lambda_{\mathbf{S}}}}. \quad (28)$$

The lefthand expression gives a necessary condition for a trajectory to slide from  $\beta = \beta_{\mathbf{S}}$  to  $\beta = \beta_{\mathbf{N}}$  along  $\Sigma_{\mathbf{N}}$ ; the righthand expression gives a necessary condition for a trajectory to slide from  $\beta = \beta_{\mathbf{N}}$  to  $\beta = \beta_{\mathbf{S}}$  along  $\Sigma_{\mathbf{S}}$ . Since the crossing points  $\beta_{\mathbf{N}}$  and  $\beta_{\mathbf{S}}$  lie on the intersections of  $\Sigma_{\mathbf{N}}$  and  $\Sigma_{\mathbf{S}}$  with  $\Sigma$ , we have also

$$|\beta_{\mathbf{N}}| = \frac{1}{\sqrt{\sigma_{\mathbf{N}}}}, \quad |\beta_{\mathbf{S}}| = \frac{1}{\sqrt{\sigma_{\mathbf{S}}}}. \quad (29)$$

Equations (28)-(29) are necessary for a periodic orbit. It remains to solve (28)-(29) for the unknown complex constants  $\beta_{\mathbf{N}}$  and  $\beta_{\mathbf{S}}$ . We must also demand that the orbit is a solution of the piecewise-smooth system for all times  $\tau$ , by verifying that  $|\beta(\tau)| \geq 1/\sqrt{\sigma_{\mathbf{N}}}$  for the orbit from  $\beta_{\mathbf{S}}$  to  $\beta_{\mathbf{N}}$ , and  $|\beta(\tau)| \leq 1/\sqrt{\sigma_{\mathbf{S}}}$  for the orbit from  $\beta_{\mathbf{N}}$  to  $\beta_{\mathbf{S}}$ .

A schematic diagram of the flow in phase space is given in Figure 7, with a periodic orbit depicted inset in 7(i).

## C. Conditions for catastrophic grazing-sliding

A grazing-sliding bifurcation takes place when a sliding orbit in  $\Sigma_{\mathbf{N}}$  or  $\Sigma_{\mathbf{S}}$  grazes the intersection with  $\Sigma$ , that is, that  $\dot{\Theta} = 0$  when the orbit crosses  $\Theta = 1$ . The  $\dot{\Theta}$  nullcline of sliding orbits is given by

$$\operatorname{Im}\beta = |\beta|^2 \operatorname{Re}\Lambda_r \quad (30)$$

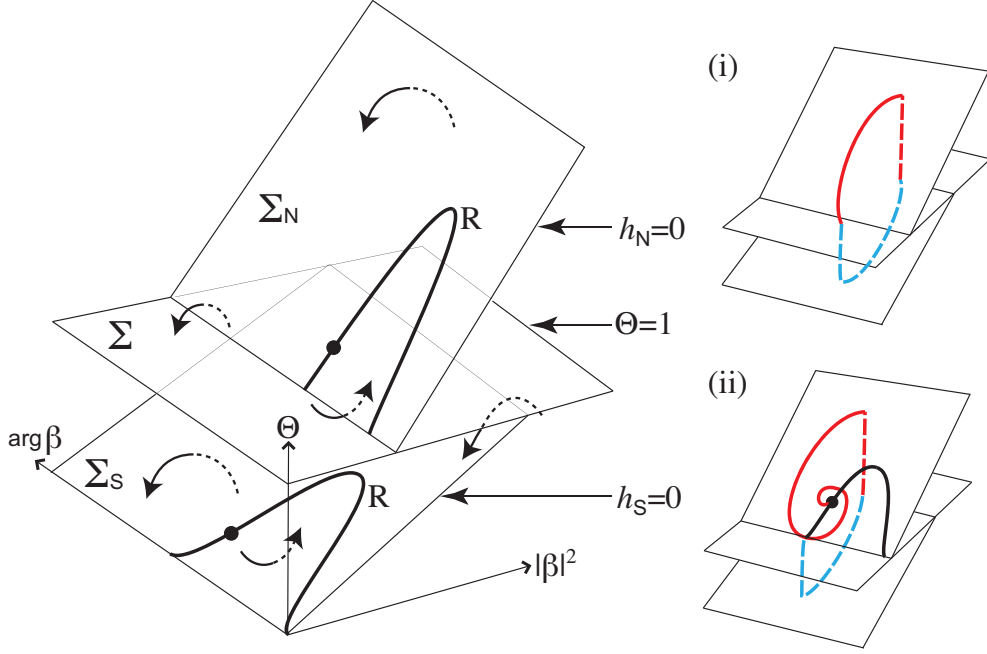


FIG. 7: (Color online) Geometry of the stripline resonator model. The switching manifold  $\Sigma$  and slow manifolds  $\Sigma_{N,S}$  are shown. Arrows indicate flow directions in the original system (8), in which the flow changes radial direction through  $\Sigma_{N,S}$  at the bold curves  $R$ , which transect  $\Sigma$  at the condition (32). Black dots are the equilibria (23). Inset: illustrations of (i) a periodic orbit, and (ii) catastrophic grazing-sliding bifurcation of a periodic orbit.

shown as the curve  $R$  in Figure 7, which crosses  $\Sigma$  when  $\Theta = 1 = \sigma_r |\beta|^2$ . Thus sliding orbits graze  $\Sigma$  at

$$\beta_r = \frac{1}{\sigma_r} \left( \pm \sqrt{\sigma_r - (\text{Re}\Lambda_r)^2} + i\text{Re}\Lambda_r \right) \quad (31)$$

if and only if the term under the square root is positive. Considering that catastrophic grazing requires the orbit tangent to  $\Sigma$  to be an admissible solution of (10) – typically called *visible* grazing – and assuming that it occurs on the branch of (31) where equilibria can occur, we find that catastrophic grazing can occur in the region  $r = N, S$  at

$$\beta_r^{graz} = \frac{1}{\sigma_r} \left( \text{sign}(\text{Im}\Lambda_r) \sqrt{\sigma_r - (\text{Re}\Lambda_r)^2} + i\text{Re}\Lambda_r \right) \quad (32)$$

provided that the region  $r$  contains an admissible equilibrium (conditions (24) or (25)). A periodic orbit undergoing catastrophic grazing in region  $N$  is illustrated in Figure 7(ii).

## V. NUMERICAL ANALYSIS

Numerical illustrations of this analysis follow. The results were found using a combination of Mathematica [26] to produce the simulations in Figure 9 and to find periodic solutions at isolated parameters, and the continuation software AUTO [27] to trace the bifurcation of that solution as parameters vary.

In Figure 8 we present two-dimensional bifurcation diagrams for the system in the parameter space  $(\omega_p, |b^{\text{in}}|^2)$  for different values of  $\omega_{0\text{N}}$ . Figure 8(iii), in particular, is qualitatively comparable with experimental results such as in [17]. This is followed by numerical simulations to illustrate the typical dynamics throughout parameter space.

Recalling the importance of the driving amplitude  $|b^{\text{in}}|^2$  and frequency  $\omega_p$  in equation (5), which enter the preceding analysis through the quantities  $\text{Im}\Lambda$  and  $\sigma$  defined in (6), it is convenient to plot quantities  $P = \frac{4\hbar}{g^3(T_C - T_0)C} |b^{\text{in}}|^2$  (proportional to pump power) and  $w = \omega_p/g$ . These are related to the dimensionless parameters by

$$P = \sigma_r / (\omega_{0r} \gamma_1 \gamma_{2r}) \quad w = \text{Im}\Lambda_r + \omega_{0r}/g \quad (33)$$

and give different curves for  $r = \text{N}$  and  $\text{S}$ . In Figure 8 we plot  $P$  against  $w$ , showing the zones where stable fixed points exist, bounded by the solid red ( $\text{N}$ ) and blue ( $\text{S}$ ) parabolas given by (24) and (25), previously identified in [16]. Also shown are the bifurcation curves of catastrophic grazing in the  $\text{N}$  region (dotted red curve) or  $\text{S}$  region (dotted blue curve). These are numerical solutions of the periodic orbit conditions (28)-(29) with the visible grazing condition (32). (Spurious curves of inadmissible solutions, which are numerous and easy to find, are of course discarded).

Figure 8(i) is symmetric in a vertical line through the parabolae, displaying the relation that if an orbit  $\beta(\tau)$  is a solution of a system with parameters  $\Lambda_{\text{N}}, \Lambda_{\text{S}}, \sigma_{\text{N}}, \sigma_{\text{S}}$ , then the orbit  $-(\beta(\tau))^*$  is a solution of a system with parameters  $\Lambda_{\text{N}}^*, \Lambda_{\text{S}}^*, \sigma_{\text{N}}, \sigma_{\text{S}}$ , where  $*$  denotes the complex conjugate.

Numerical solutions for the catastrophic grazing bifurcation curves fail when they lie close to the parabolic curves bounding stability zones. However, further simulations not shown here confirm that they form closed continuous curves, approaching the parabolae and contacting them tangentially at isolated points, where  $\text{Im}\Lambda_r = 0$  and hence  $\Lambda_r = \sqrt{\sigma_r}$ . The curves consist of two smooth branches: catastrophic grazing-sliding bifurcations occur in

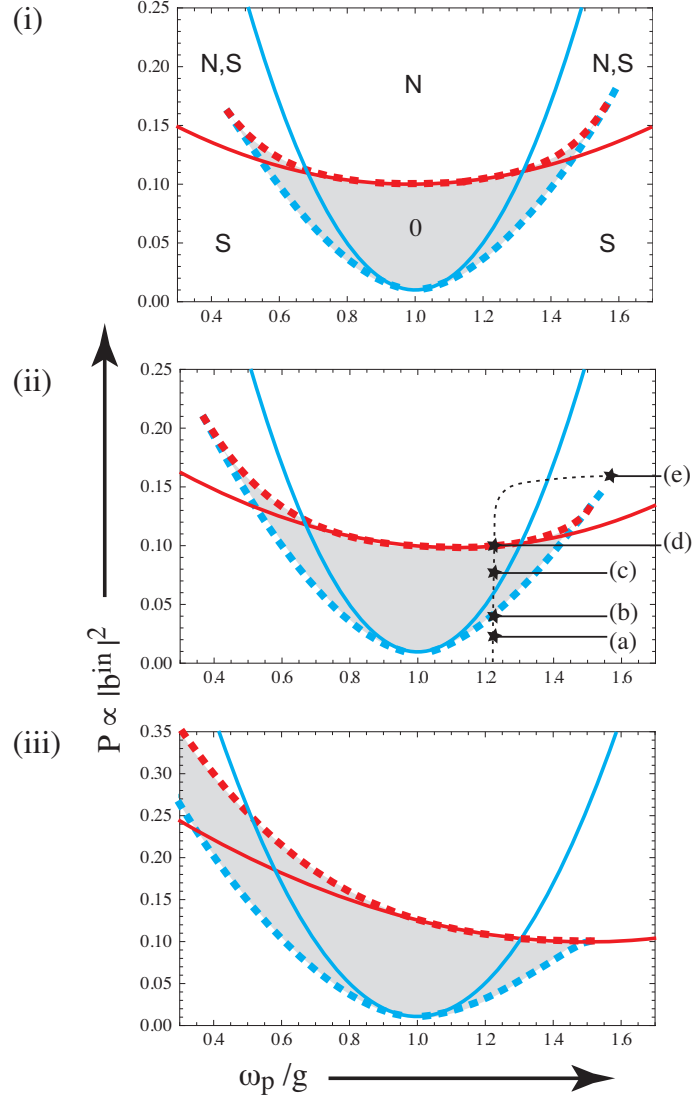


FIG. 8: (Color online) Plot of  $P \propto |b^{\text{in}}|^2$  against  $w = \omega_p/g$  as given by (33) for  $\text{Re}\Lambda_S = -0.1$ ,  $\text{Re}\Lambda_N = -1$ ,  $\omega_{0S}\gamma_1\gamma_{2S} = 1$ ,  $\omega_{0N}\gamma_1\gamma_{2N} = 0.1$ ,  $\omega_{0S}/g = 1$ , where  $\omega_{0N}/g$  takes values: (i) 1, (ii) 1.1, (iii) 1.5. N indicates the admissible equilibrium in existence above the red full parabola given by (24), S indicates the admissible equilibrium existing below the blue full parabola given by (25), elsewhere 0 denotes no equilibria. A periodic orbit exists in the shaded zone bounded by the bifurcation curves of catastrophic grazing-sliding in N (red/upper dotted curve) or S (blue/lower dotted curve).

N along the upper dotted curve and in S along the lower dotted curve. The curves tend towards intersection points in the bistable zones, which are codimension two points where a periodic orbit simultaneously grazes in both the N and S regions.

Figure 9 depicts simulations that illustrate the evolution of the system through parameter

space, as we follow the dotted curve through points labelled (a)-(e) in Figure 8(ii). Here we plot phase portraits in the complex  $\beta$  plane. The inner circle is where orbits on  $\Sigma_{\mathbf{N}}$  switch into region  $\mathbf{S}$ , and the red curves are orbits on  $\Sigma_{\mathbf{N}}$ . Similarly, the outer circle is where orbits on  $\Sigma_{\mathbf{S}}$  switch into region  $\mathbf{N}$ , and the blue curves are orbits on  $\Sigma_{\mathbf{S}}$ .

Starting on the dotted line in Figure 8(ii) near  $P = 0$ , the system has an equilibrium in the  $\mathbf{S}$  region. The vector fields (20) are nowhere tangent to the switching manifold  $\Sigma$ . Moving up the line, as we pass the value of  $P$  level with the apex of the narrower (blue) parabola, there appears a cubic tangency of the sliding vector field  $F_{\mathbf{S}}$  to  $\Sigma$ , which splits into two quadratic tangencies. This happens because the curve  $\mathbf{R}$  below  $\Sigma$  in Figure 7 expands to touch  $\Sigma$  and thereafter intersects it twice. No periodic orbit exists and all trajectories go to the equilibrium as shown in Figure 9(a). At the bifurcation curve a periodic orbit with finite period appears by a catastrophic bifurcation, shown in Figure 9(b); at grazing a trajectory may evolve either along the periodic orbit or towards the equilibrium. Passing through the narrower parabola, equation (25) is violated so the equilibrium in  $\mathbf{S}$  becomes inadmissible, as in Figure 9(c).

Moving up the line, as we pass the value of  $P$  level with the apex of the wider (red) parabola, there appears a cubic tangency of the sliding vector field  $F_{\mathbf{N}}$  to  $\Sigma$ , which splits into two quadratic tangencies as the curve  $\mathbf{R}$  appears above  $\Sigma$  in Figure 7 and thereafter intersects it twice. Then passing from the astable zone (where no equilibria are admissible) through the wider parabola, equation (24) is satisfied so the equilibrium in  $\mathbf{N}$  becomes admissible. Very nearby the limit cycle undergoes the catastrophic grazing-sliding bifurcation by grazing in region  $\mathbf{N}$ , shown in Figure 9(d) where, in fact, the grazing point and boundary equilibrium are too close to resolve. Moving on to the zone above all bifurcation curves, an equilibrium exists in  $\mathbf{N}$  and the periodic orbit does not exist. If we pass again through the narrower parabola, by varying  $\omega_p/g$ , we satisfy equation (25), so the equilibrium in  $\mathbf{S}$  becomes admissible, returning to the scenario in Figure 9(a). The point (e) represents the codimension two point where catastrophic grazing curves intersect. Following our path, a limit cycle appears with finite amplitude, simultaneously grazing in both regions  $\mathbf{N}$  and  $\mathbf{S}$ . From this point a generic perturbation takes us either into the region inside the bifurcation curves where the periodic orbit exists, or outside where it vanishes.

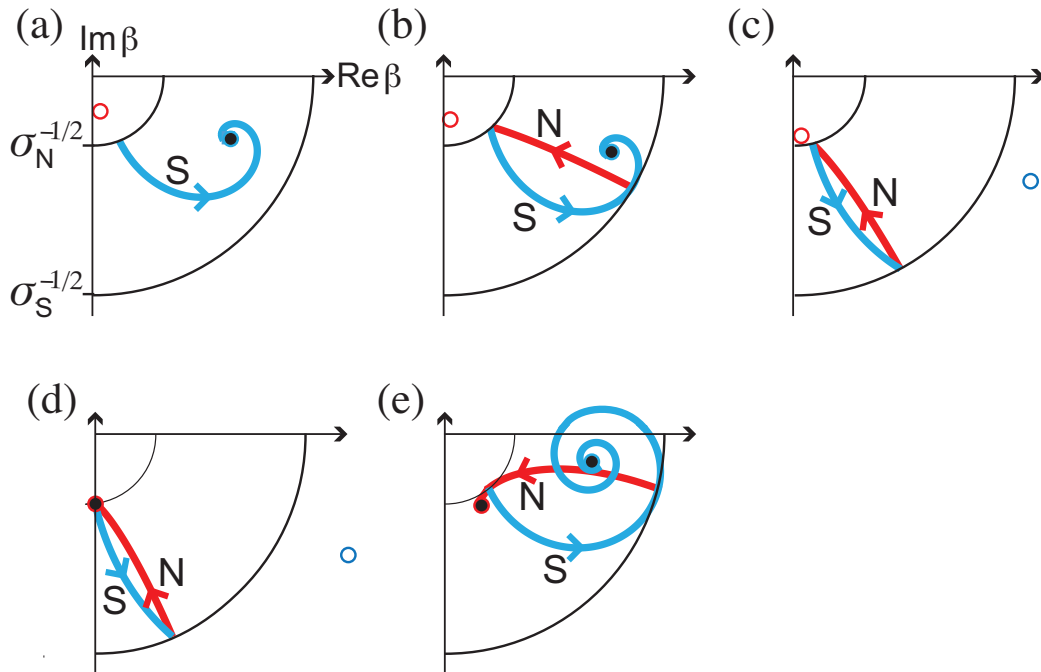


FIG. 9: (Color online) Simulations at the points (a)-(e) in Figure 8(ii), showing the  $-\frac{\pi}{4} < \arg \beta < 0$  quadrant of the complex  $\beta$  plane. The circular arcs are the switching boundaries  $|\beta|^2 = 1/\sigma_N$  and  $|\beta|^2 = 1/\sigma_S$ , the orbits belong to N (red) or S (blue) are labeled. Filled circles are admissible equilibria, empty circles are inadmissible. The cases are: (a)  $w = 1.22$ ,  $P = 0.026$ , showing an equilibrium in region S; (b)  $w = 1.22$ ,  $P = 0.039$ , showing grazing in S, a periodic orbit appears in a catastrophic grazing-sliding bifurcation; (c)  $w = 1.22$ ,  $P = 0.079$ , the periodic orbit in the stable zone; (d)  $w = 1.22$ ,  $P = 0.101$ , showing a periodic orbit homoclinic to the equilibrium of N; (e)  $w = 1.58$ ,  $P = 0.165$ , showing the codimension two scenario where the bifurcation curves meet in the bistable zone, implying catastrophic grazing-sliding simultaneously at both switching boundaries.

## VI. CONCLUDING REMARKS

We have introduced what is, to our knowledge, the first thorough description of a catastrophic case of sliding bifurcation in a piecewise-smooth system. We have given its definition and the conditions for it to occur.

We have shown that catastrophic grazing-sliding of a periodic orbit occurs in an experimentally motivated model of a superconducting stripline resonator, where it forms the mechanism for sudden destruction of oscillatory modes. The simulations and bifurcation

diagram in Section V qualitatively match experimental transitions observed in [17] as pump power is increased, although noise will affect the precise dynamics near the boundaries where fixed points appear/disappear. The mechanism is therefore a viable explanation for the sudden collapse from periodicity to stable states observed in the power output of the physical system. We have not described the behaviour of the model fully, using it only to illustrate in detail the role of catastrophic grazing-sliding in this context. However, we have shown the simplicity of the qualitative behaviour revealed by deriving grazing conditions, such as those leading to Figure 7.

A detailed investigation of the catastrophic grazing-sliding bifurcation in the original slow-fast model is beyond the scope of this paper, however, the periodic orbit simulated here corresponds closely to that observed in previous numerical simulations of the slow-fast model [17]. For completeness we present, in Figure 10, a comparison of Figure 8(iii) to a numerical solution for a smoothed out system, based on the slow-fast system in equation (8) with a sigmoidal smoothing of the vector field at the switching manifold  $\Sigma$ . In Figure 10, the boundary (full curve) of the zone where equilibria occur in  $S$  is reproduced precisely in the smooth model, where it is a curve of folds of equilibria. The dashed bifurcation curve was found by continuation of a bifurcation that destroys a periodic orbit, and the orbit is close dynamically to that in the Filippov system. Several formally different sigmoidal functions were used and showed no difference in outcome, provided they had a sufficiently steep slope. The figure shows that near resonance, given by  $|\omega_p - \omega_0|/g \ll 1$  and therefore  $|\text{Im}\Lambda| \ll 1$ , the bifurcation curves of the smooth system show good agreement with the piecewise-smooth system. As  $|\text{Im}\Lambda|$  increases, the curves slowly diverge from each other, which is expected because the slow and fast dynamics become less distinct, so the Filippov model becomes less accurate.

It is worth emphasising that the conditions (3)-(4) for catastrophic grazing-sliding are generic in Filippov systems. Neither the slow-fast behaviour nor the tri-dimensionality of the case study are prerequisites for the bifurcation illustrated – indeed from Section III C onward we are effectively studying a one-parameter bifurcation in a planar Filippov system.

The implication is that the bifurcation is typical in piecewise-smooth systems. It is found at the boundary between crossing and repelling sliding on a switching manifold, and governs the sudden destruction of periodic orbits that is not preceded by any significant change in their stability or period.

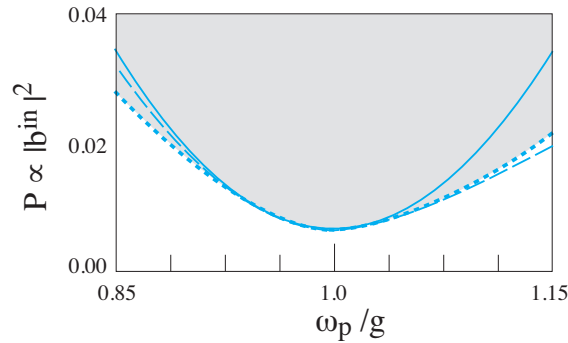


FIG. 10: (Color online) A magnification of Figure 8(iii) near resonance, showing the boundary of the S stability zone (full curve), the catastrophic grazing bifurcation curve (dotted curve). Shown for comparison is a bifurcation curve where periodic orbits vanish (dashed curve) in a smoothed version of the slow-fast system in equation (8).

### Acknowledgements

The authors wish to thank Eran Segev and Eyal Buks for helpful comments and source materials. This work is based in part upon work by SWS supported by the National Science Foundation under Grant Number CMMI-0758419, and by MRJ supported by the EPSRC and by a Royal Society International Travel Grant.

- 
- [1] B. Brogliato. *Impact in mechanical systems - analysis and modelling*, volume 551 of *Lecture Notes in Physics*. Springer-Verlag (New York), 2000.
  - [2] K. Popp and P. Shelter. Stick slip vibrations and chaos. *Phil. Trans. Roy. Soc. A*, 332(1624):89–105, 1990.
  - [3] S. Banerjee and G. Verghese. *Nonlinear phenomena in power electronics*. IEEE press (New York), 2001.
  - [4] M. diBernardo, F. Garofalo, L. Glielmo, and F. Vasca. Switchings, bifurcations, and chaos in dc/dc converters. *IEEE Trans. Circuits Syst. I*, 45:133–141, 1998.
  - [5] M. diBernardo, K. H. Johansson, and F. Vasca. Self-oscillations and sliding in relay feedback system: symmetry and bifurcations. *Int.J.Bif.Chaos*, 11(4):1121–1140, 2001.
  - [6] R. Casey, H. de Jong, and J. L. Gouze. Piecewise-linear models of genetic regulatory networks: Equilibria and their stability. *J.Math.Biol.*, 52:27–56, 2006.

- [7] B. Brogliato. *Nonsmooth mechanics – models, dynamics and control*. Springer-Verlag (New York), 1999.
- [8] M. diBernardo, C. J. Budd, A. R. Champneys, and P. Kowalczyk. *Piecewise-Smooth Dynamical Systems: Theory and Applications*. Springer, 2008.
- [9] R. I. Leine and N. Henk. *Dynamics and Bifurcations of Non-Smooth Mechanical Systems*. Springer, 2004.
- [10] A. J. van der Schaft and J. M. Schumacher. *An introduction to hybrid dynamical system*. Springer-Verlag (New York), 2000.
- [11] A. F Filippov. *Differential Equations with Discontinuous Righthand Sides*. Kluwer Academic Publishers, Dordrecht, 1998.
- [12] M. diBernardo, P. Kowalczyk, and A. Nordmark. Bifurcations of dynamical systems with sliding: derivation of normal-form mappings. *Physica D*, 170:175–205, 2002.
- [13] M. diBernardo, P. Kowalczyk, and A. Nordmark. Sliding bifurcations: a novel mechanism for the sudden onset of chaos in dry friction oscillators. *Int.J.Bif.Chaos*, 10:2935–2948, 2003.
- [14] M. R. Jeffrey and S. J. Hogan. The geometry of generic sliding bifurcations. *SIREV*, submitted 2009.
- [15] D. V. Turaev and L. P. Shilnikov. Blue sky catastrophes. *Dokl. Math.*, 51:404–407, 1995.
- [16] E. Segev, B. Abdo, O. Shtempluck, and E. Buks. Thermal instability and self-sustained modulation in superconducting NbN stripline resonators. *J. Phys: Condens. Matter*, 19(9):096206(14pp), 2006.
- [17] G. Bachar, E. Segev, O. Shtempluck, E. Buks, and S. W. Shaw. Noise induced intermittency in a superconducting microwave resonator. *arXiv:0810.0964*, 2008.
- [18] E. Segev, B. Abdo, O. Shtempluck, and E. Buks. Novel self-sustained modulation in superconducting stripline resonators. *EPL*, 78(5):57002 (5pp), 2007.
- [19] E. Segev, B. Abdo, O. Shtempluck, and E. Buks. Extreme nonlinear phenomena in NbN superconducting stripline resonators. *Physics Letters A*, 366(1-2):160 – 164, 2007.
- [20] L. E. Kollar, G. Stepan, and J. Turi. Dynamics of piecewise linear discontinuous maps. *Int.J.Bif.Chaos*, 14(7):2341–2351, 2004.
- [21] T. LoFaro. Period-adding bifurcations in a one parameter family of interval maps. *Mathematical and Computer Modelling*, 24:27–41, 1996.
- [22] H. Lamba. Chaotic, regular and unbounded behavior in the elastic impact oscillator. *Physica*

- D*, 82(1-2):117–135, 1995.
- [23] S. W. Shaw and P. J. Holmes. Periodically forced linear oscillator with impacts: Chaos and long-period motions. *Phys. Rev. Lett.*, 51:623–626, 1983.
- [24] P. Kowalczyk and M. diBernardo. Two parameter degenerate sliding bifurcations in Filippov systems. *Physica D*, 204:204–229, 2005.
- [25] N. Fenichel. Geometric singular perturbation theory. *J. Differential Equations*, 31:53–98, 1979.
- [26] S. Wolfram. *The Mathematica Book*. Cambridge University Press, 1996.
- [27] E. J. Doedel, A. R. Champneys, T. F. Fairgrieve, Yu. A. Kuznetsov, B. Sandstede, and X. Wang. AUTO97: Continuation and bifurcation software for ordinary differential equations (with HomCont). *Technical report, Concordia University*, 1997.